Original Paper

Unlocking the potential of V/Ti-AAC: a promising eco-friendly catalyst for cyclohexene epoxidation

Noureddine Belaidi[1], Hajer Azzi[1,2], Sanaa El-Korso[1], Abderrahim Choukchou-Braham[1] and

Abdelkader Nebatti-Ech Chergui[3]

[1]Laboratoire de Catalyse et Synthèse en Chimie Organique, Faculté des Sciences, Université de Tlemcen, Algérie; [2]Université de Ain Temouchent, Faculté des Sciences et de la Technologie, BP 284,46000 Ain Témouchent, Algérie and [3]Laboratory of Applied Hydrology and Environment, University of Ain-Temouchent Belhadj Bouchaib, Faculty of Sciences and Technology, Algeria

Abstract

Bentonite is an abundant natural resource in the Maghnia region of Algeria that may have potential value in catalysis, but heretofore has been considered of low value for this purpose due to its low acidity and low catalytic activity. Low cost is one of the main criteria for choosing a suitable material for catalysis. Because bentonite is abundant and low-cost, its use as a starting material for the preparation of catalysts deserves reconsideration. The present study was undertaken, therefore, to optimize the performance of bentonite as a catalyst in one of the most promising reactions in organic synthesis, namely, cyclohexene epoxidation. The bentonite was subjected to adjustment of its structure by means of a number of laboratory treatments based on its large cation exchange capacity. These modifications aimed to achieve an environmentally friendly catalytic process by incorporating transition metals, specifically titanium and vanadium, into the modified bentonite structure through acid activation. Redox properties were enhanced and Lewis and Brønsted acidities were introduced. The vanadium oxide, supported on titania-pillared, acid-activated bentonite (5V/Ti-AAC), was characterized comprehensively using various techniques, including diffuse-reflectance UV-visible spectroscopy (DR UV-Vis), Fourier-transform infrared spectroscopy (FTIR) for surface acidity analysis, X-ray diffraction (XRD), nitrogen adsorption-desorption isotherms, and scanning electron microscopy (SEM) coupled with energy-dispersive X-ray elemental analysis (EDX). The catalytic activity was investigated in response to certain variables, such as catalyst mass, nature of the solvent, amount of oxidant, and reaction temperature. A kinetic study was conducted to understand the reaction behavior. The experimental results demonstrated intriguing catalytic activity, achieving a 42% conversion rate with ~68% selectivity toward the epoxide product when employing tert-butyl hydroperoxide (TBHP) as the oxidant and heptane as the solvent. This study highlights the potential of 5V/Ti-AAC as an environmentally friendly catalyst applied in the epoxidation of cyclohexene.

Keywords: Bentonite; Cyclohexene; Epoxidation; Titanium; Vanadium

Introduction

Clay minerals are currently commonly employed in catalysis because they are inexpensive, abundant in nature, and environmentally friendly. However, their usefulness is restricted due to a lack of porosity and low thermal stability. As a result, adjustments are made to improve these properties, including acid treatment and the pillaring process (Bineesh et al., 2010b). Acid treatment is a useful approach in enhancing the catalytic activity of clay minerals (Komadel and Madejová, 2006). Acid-modified clay minerals are being used widely in the following ways: disposal of radioactive waste (Wang et al., 2010); removal of heavy metals from industrial

wastewaters (Oubagaranadin et al., 2010); and as catalysts or catalyst supports (Chitnis and Sharma, 1997; Rhodes et al., 1991). On the other hand, the pillaring process, during which rigid metal-oxides are inserted or intercalated between the clay mineral layers, increases the specific surface area of the solid which improves the performance of low-surface-area catalysts by adding to the pillared interlayer clays (PILC) (Torres et al., 2021). PILC materials, thus, have attracted much interest and are an active research subject (Centi and Perathoner, 2008; Najafi et al., 2021; Pinnavaia, 1983). Several studies have been devoted to PILCs, reviewing various aspects of their preparation, characterization, and application. Because of their porosity, thermal stability, acidity, and reactivity, PILCs are used widely as catalysts or supports for catalytic materials and applied in several chemical processes (Centi and Perathoner, 2008; Huang et al., 2010; Pinnavaia, 1983). Recently, many studies have shown that vanadia supported on Ti-pillared clay (V/Ti-PILC) is more active than Ti-PILC in various reactions such as selective catalytic oxidation of H_2S (Bineesh et al., 2009); ammoxidation of m-xylene (Bahranowski

Corresponding authors: N. Belaidi and A. Nebatti-Ech Chergui; Emails: belaidi.doc2014@gmail.com, abdelkader.nebatti@univ-temouchent.edu.dz

et al., 1995), selective catalytic reduction of NO by NH$_3$ (Bahranowski et al., 1997; Chae et al., 2004; Long and Yang, 2000a), oxidative dehydrogenation of propane (Bahranowski et al., 2000), and epoxidation of allylic alcohol over vanadium-supported Ti-pillared clay (Arfaoui et al., 2010). Epoxidation reactions are one of the key reactions in the chemical industry promoting the conversion of olefins into oxygenated molecules, referred to as epoxides, by an oxygen transfer reaction. Epoxides are important and versatile commercial intermediates used as key raw materials for a wide variety of products due to the many reactions they can undergo (Sreethawong et al., 2005). The epoxidation of cyclohexene to yield cyclohexene oxide as the main product is one of the most difficult to achieve of these types of reactions, for two main reasons, i.e. allylic oxidation and epoxy ring opening occur readily and interfere with epoxidation (El-Korso et al., 2014). Cyclohexene oxide is an important organic intermediate used in the production of pharmaceuticals, plant protection agents, pesticides, and stabilizers for chlorinated hydrocarbons (Gao et al., 2004; Parida and Mallick, 2009). Much effort is invested in the development of novel active and selective cyclohexene epoxidation catalysts that avoid side reactions and the subsequent formation of large amounts of unwanted by-products (El-Korso et al., 2016). In an attempt to enhance the catalytic performance of bentonite, the present study aimed to address the inefficiency of bentonite as a catalyst due to its low acidity and low catalytic activity by first exposing it to acid treatment then incorporating transition metals, specifically titanium and vanadium, in order to impart to it Brønsted and/or Lewis acidity and oxidation-reduction properties. A further objective was to understand better the correlation between the physicochemical properties of this catalyst and its performance in the epoxidation of cyclohexene.

Materials and methods

Raw materials and preparation of catalysts

In the present study, a Maghnia (Algeria) bentonite was utilized as the primary clay material. Before its application, the raw bentonite underwent a purification process (120 g of bentonite was dispersed in 1.5 L of distilled water in a 5 L beaker with stirring for 15 min). Then, a buffer solution (0.3 M sodium citrate, Hebei Fengqiang Trading, China, 99%), 1 M sodium bicarbonate, and 2 M sodium chloride (Aldrich, 99%) at pH = 7.3 was added to the bentonite. After that, the mixture was heated with stirring at a temperature of 75°C for 20 min. 15 g of sodium thiosulfate, Na$_2$S$_2$O$_3$(Prolabo, 99%), was then added slowly. After 15 min of stirring, a further 15 g of Na$_2$S$_2$O$_3$ (Prolabo, 99%) was added. The cooled mixture was centrifuged using a Rotofix 32A Hettich centrifuge (Andreas Hettich, Germany), at (6000 rpm, 4226×*g*) for 15 min. The bentonite was washed twice with 0.05 M HCl (1.5 L) (Biochem Chemopharma, Cosne-Cours-sur-Loire, France, 37%) for 3–4 h. After centrifugation (6000 rpm, 4226×*g*), the bentonite was redispersed in 2.5 L of hydrogen peroxide (H$_2$O$_2$: 10 volumes) (Sigma-Aldrich, 30%) overnight, then heated at 70°C for 30 min to remove the organic matter. The cation exchange capacity (CEC) was measured in a previous study (Belaidi et al., 2015) by exchanging cobalthexamine cations (Aldrich, 99%), then analyzed by UV-vis using the procedure of Ciesielski and Sterckeman (1997), to be 95 meq g^{-1} and the basal spacing was also determined by Belaidi et al. (2015) by XRD to be 13.8 Å. To produce the acid-activated clay, referred to as AAC, the initial bentonite was dispersed in a 1.0 M HCl solution (Biochem

Chemopharma, 37%, France) and stirred vigorously at 80°C for 4 h. The resulting AAC material was then modified by the incorporation of Ti polycations as pillars, following the procedure of Yamanka et al. (1987). Following incorporation of Ti, the solid was separated by centrifugation using a Rotofix 32A Hettich centrifuge (Andreas Hettich, Germany) at (6000 rpm, 4226×*g*) and subsequently dried at 80°C for 16 h. To obtain Ti-pillared, acid-activated clay, denoted as Ti-AAC, the material was finally calcined at 400°C for 3 h. The method of Bahranowski et al. (1995) was followed to prepare the material with 5% mass of vanadium. Then, it was dried at 80°C for 20 h and calcined at 500°C for 5 h. The catalyst prepared was referred to thereafter as 5V/Ti-AAC.

Characterization methods

The 5V/Ti-AAC samples were characterized using various techniques. X-ray powder analysis (XRD) was performed using a Rigaku D/max 2500 diffractometer (Rigaku Corporation, Japan) using Ni-filtered CuKα radiation (λ = 1.541874 Å). The scanning range was between 2.5 and 70°2θ at a scanning speed of 0.03°2θ/s. Prior to analysis the samples were ground to fine powder. N$_2$ adsorption-desorption analysis was conducted using a Quantachrome Nova 1000e instrument (Quantachrome Corporation, France) to determine the specific surface area, pore volume, and micropore volume. The pore-size distribution was calculated using the Barret-Joyner-Halenda (BJH) method for the desorption branch (Bardestani et al., 2019), and the micropore volume and micropore surface area were calculated by the t-plot-de Boer method (Lippens and de Boer, 1995). Prior to physisorption measurements, the samples were outgassed at 250°C for 3 h under vacuum.

Diffuse-reflectance UV-visible (UV-Vis) spectra in the range 200–800 nm were obtained using a Perkin-Elmer Lambda 800 UV-Vis spectrometer (PerkinElmer, Massachusetts, USA). The samples in powder form were placed in the sample holder and the baseline was established using BaSO$_4$ as a reference. Fourier-transform infrared spectroscopy (FTIR) analysis was conducted at room temperature using a Cary 600 FTIR spectrometer (Agilent Technologies, California, USA). The modified bentonite materials were dried in a hot air oven at 100°C for 1 h before pyridine treatment in order to remove moisture. Then, the samples were placed in direct contact with pyridine (Aldrich, 99.8%). Prior to FTIR measurements the samples were heated in an oven at 120°C for 1 h in order to remove the physisorbed pyridine. The FTIR spectra were recorded over the spectral range 1650–1350 cm^{-1} at a resolution of 4 cm^{-1}, using KBr as a background. Finally, the scanning electron microscopy (SEM) with energy-dispersive X-ray elemental analysis (EDX) was performed using a Hitachi-TM1000 instrument (Elexience, France) at an acceleration voltage of 150 kV.

Catalytic experiments

The catalytic epoxidation of cyclohexene (Labosi, 99%, France) was carried out using tert-butyl hydroperoxide, TBHP (Sigma Aldrich, 70 wt.% in H$_2$O, France), as the oxidant in a two-neck, glass, round-bottom flask equipped with a magnetic stirrer and reflux condenser. Initially, 20 mL of solvent and 38.45 mmol (5.5 mL) of TBHP were combined in a closed Erlenmeyer flask and stirred magnetically for 24 h. Afterward, the organic phase was separated from the aqueous phase. Subsequently, 29 mmol (3 mL) of cyclohexene was added to the TBHP-solvent mixture. The reaction mixture was heated to 65°C with vigorous stirring, and then the catalyst (100 mg) was

introduced at time zero. The progress of the reaction was monitored using gas chromatography (GC) with a Shimadzu GC 14-B instrument (Shimadzu, France) equipped with an Agilent HP-FFAP capillary column and a flame ionization detector (FID). The remaining TBHP was determined by iodometric titration of the organic phase at the end of the reaction.

$$\text{Conversion}\,(\%) = \frac{[C_6H_{10}]_0 - [C_6H_{10}]_t}{[C_6H_{10}]_0} \times 100 \quad (1)$$

$$\text{Selectivity}\,(\%) = \left[\frac{\text{moles individual product}}{\text{moles of converted cyclohexene}}\right] \times 100 \quad (2)$$

$$\text{TOF}\,(\text{h}^{-1}) = \frac{\text{number of epoxide molecules}}{\text{number of V sites} \times \text{time}} \quad (3)$$

where TOF = turnover frequency.

Results and discussion

Materials characterization

The XRD patterns of the AAC, Ti-AAC, and 5V/Ti-AAC samples (Fig. 1) revealed the d_{001} basal spacing for AAC at 6°2θ to be 14.7 Å (Table 1), indicating that the periodic structure of the 2:1 layers remained largely intact following the acid treatment. (Bailey et al., 1980). On the other hand, this basal spacing was absent from the XRD pattern for the Ti-AAC pillared acid-activated clay (Table 1), indicating that the layer structure was less well ordered. Clearly, the intercalation process by the small, hydrolyzed Ti moiety yielded non-uniform interlayer distances or perhaps even a delaminated structure (Chen et al., 2012; Yuan et al., 2006).

The XRD pattern for the Ti-AAC also revealed a reflection at 19–20°2θ attributed to the sum of the indices *hk* (02) and (11), and that at 35°2θ to the sum of the indices *hk* (13) and (20). The reflection at 25.3°2θ corresponds to TiO$_2$ anatase (Bineesh et al., 2010b; Chaker et al., 2020; Long and Yang, 2000b).

The XRD data for 5V/Ti-AAC are similar to those of Ti-AAC. No reflection representing vanadium oxide was observed; vanadium oxide

Table 1. Basal spacing of based clay materials

Material	Basal spacing (d_{001})
AAC	14.7 Å
Ti-AAC	–
5V/Ti-AAC	–

appears only if the vanadium loading exceeds 15% according to Long and Yang (2000b).

The adsorption and the adsorption-desorption isotherms of the AAC, Ti-AAC, and 5V/Ti-AAC (Fig. 2) are of type IV (IUPAC classification), which are indicative of mesoporous materials (Azzi et al., 2012, 2020). Moreover, during the pillar formation of Ti-AAC (Fig. 2), the slope of the adsorption-desorption isotherm increased at relatively low pressures. The materials investigated exhibited a monomodal pore-size distribution, with an average diameter ranging from 3.6 to 3.8 nm (Fig. 2). The textural properties of the prepared materials, including BET specific surface area, pore volume, micropore volume, and pore diameter, are summarized in Table 2. An increase in specific surface area was observed, from 196 to 237 m^2 g^{-1} after Ti intercalation. This enhancement in specific surface area is attributed to the successful formation of pillars (Bineesh et al., 2008, 2009).

The considerable specific surface area of Ti-AAC facilitates the effective dispersion of vanadium. However, upon impregnation of vanadium species, a reduction in specific surface area was observed. This decrease was attributed to the partial blockage of mesopores caused by the presence of vanadium species (Azzi et al., 2012, 2020; Bineesh et al., 2008, 2009). Furthermore, a decline in the volume of micropores was observed following the impregnation of vanadium, probably resulting from the partial occlusion of Ti-AAC micropores by vanadium oxides. This phenomenon was similarly documented in the study conducted by Arfaoui et al. (2006).

The DR UV-Vis spectrum of the AAC sample (Fig. 3) exhibited a broad band centered at ~250 nm which is assigned to charge transfer at the octahedral iron sites (Fe^{3+}←O^{2-}, OH$^-$ or OH$_2$) of montmorillonite in the bentonite (Arfaoui et al., 2009).
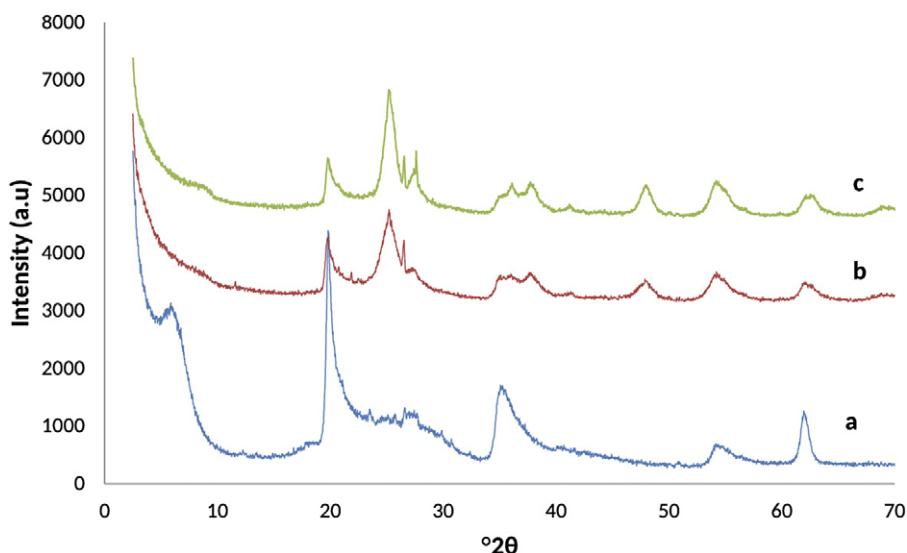

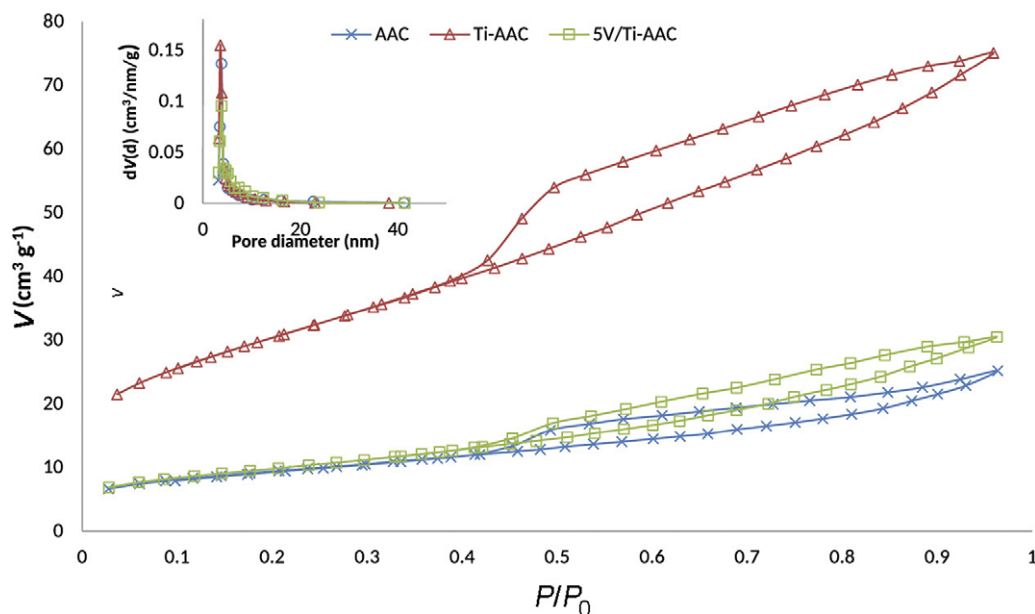**Figure 1.** XRD patterns of (a) AAC, (b) Ti-AAC, and (c) 5V/Ti-AAC.

Figure 2. N$_2$ adsorption-desorption isotherms and BJH pore-size distribution.

Table 2. Properties of the materials

	S_{BET} (m^2 g^{-1})	$S_{\mu p}$ (m^2 g^{-1})	V_t (cm^3 g^{-1})	$V_{\mu p}$ (cm^3 g^{-1})	d_p (nm)
AAC	196	72	0.237	0.039	3.8
Ti-AAC	237	93	0.256	0.052	3.6
5V/Ti-AAC	203	27	0.242	0.018	3.8

$S_{\mu p}$: micropore surface area; V_t: total pore volume; $V_{\mu p}$: micropore volume; d_p: pore diameter.

The DR UV-Vis of Ti-AAC displayed two main bands, one at 250 nm, which carried over from AAC, and the other at ~300 nm (Fig. 3), which may be due to charge transfer from the valence band (mainly formed by 2*p* orbitals of the oxide anion) to the conduction band (mainly formed by 3*d t2g* orbitals of the Ti^{4+} cations) (Bineesh et al., 2011). This band is consistent with Ti occurring in the form of anatase (Bineesh et al., 2010a, 2011).

The 5V/Ti-AAC spectrum showed three charge-transfer (CT) bands of V^{5+}: the first at ~270 nm, the second at ~350 nm, and the third at 390 nm. The band at 270 nm was assigned to the low-energy ligand-to-metal (O^{2-} to V^{5+}) charge-transfer (LMCT) transitions associated with the isolated tetrahedral monomeric V species (Concepcion et al., 2004; Iannazzo et al., 2003). The band at 350 nm was assigned to the weak chains of polymerized V involving both tetrahedral and square pyramidal configurations of V (Concepcion et al., 2004; El-Korso et al., 2015; Iannazzo et al., 2003). The band at 390 nm was assigned to (O^{2-} to V^{5+}) charge-transfer transitions associated with the isolated octahedral monomeric species (Chary et al., 2006; Held et al., 2012; Murgia et al., 2006).

The deposition or impregnation of vanadium into Ti-AAC caused a slight decrease in the main absorption intensity of the bands at 270 nm and 350 nm, which results from the disruption of the Ti-O-Ti chain by the incorporation of the vanadium species (Bineesh et al., 2010a, 2011).

The FTIR spectra over the range 1340–1640 cm^{-1} (Fig. 4) of AAC, Ti-AAC, and 5V/Ti-AAC materials before and after pyridine
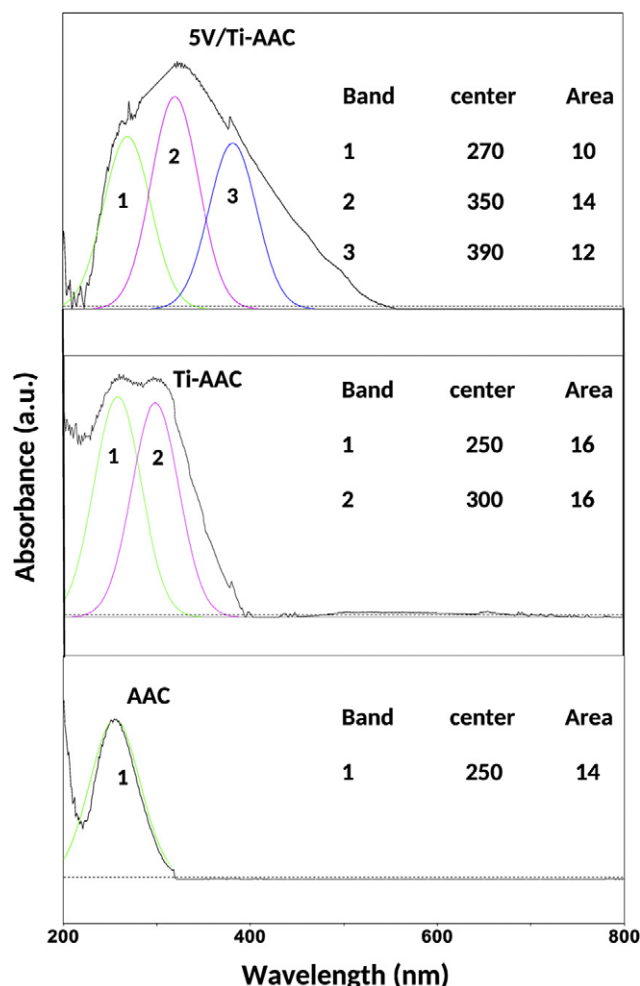

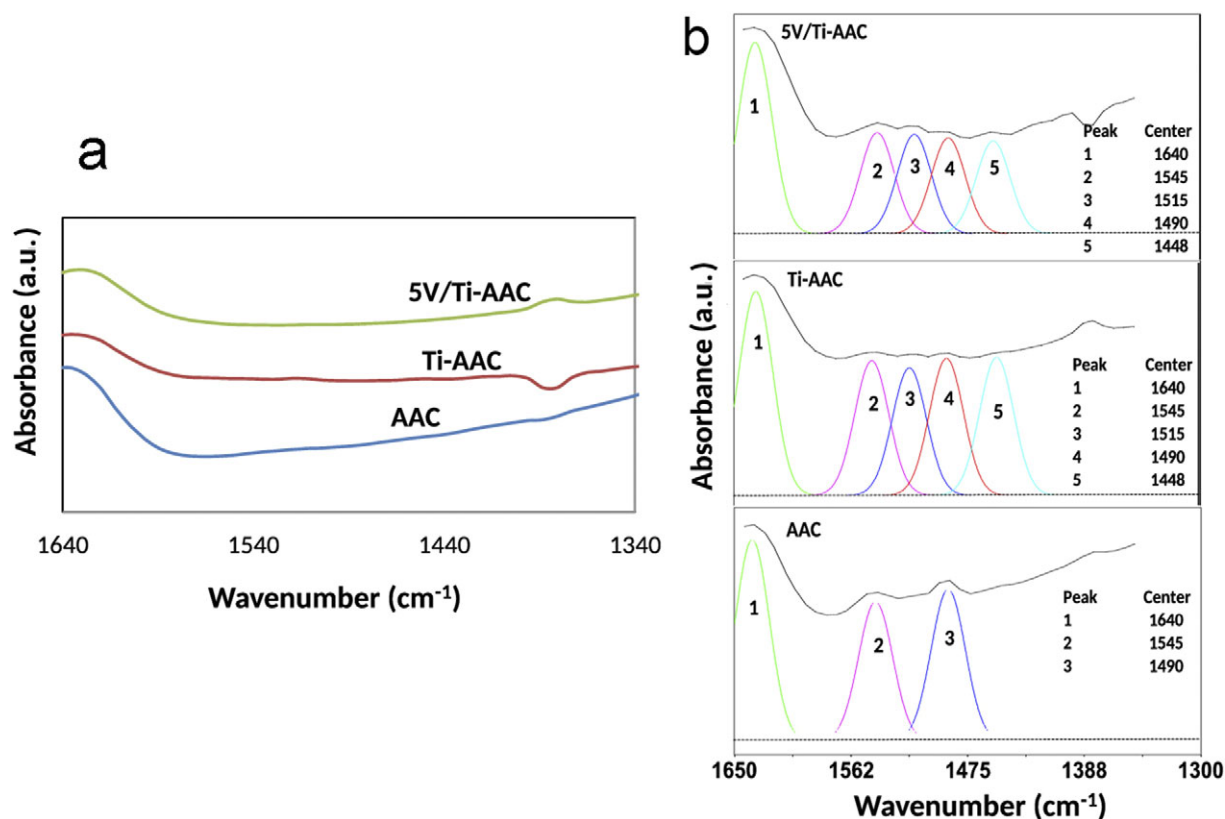**Figure 3.** DR UV-vis spectra of (a) AAC, (b)Ti-AAC, and (c) 5V/Ti-AAC.

Figure 4. FTIR spectra (a) before and (b) after pyridine adsorption.

adsorption revealed part of a broad band at ~1640 cm^{-1}, which was assumed to be from H-O-H bending vibrations from adsorbed water. Prior to pyridine treatment, no significant absorption bands were evident except for the OH groups. To remove physisorbed pyridine, the pyridine-treated samples were heated at 120°C for 1 h. No color change was observed in the materials upon pyridine treatment or after heat treatment. The FTIR spectrum of AAC displayed two distinctive bands at 1545 and 1490 cm^{-1}, corresponding to the acidic sites of Brønsted and Brønsted/Lewis, respectively (Azzi et al., 2019; Candan Karaeyvaz and Balci, 2021). The Ti-AAC spectrum shows four characteristic bands at 1545, 1515, 1490, and 1448 cm^{-1}, corresponding to the acidic sites of Brønsted, Brønsted/Lewis, and Lewis, respectively. In addition, the Ti-AAC spectrum shows the appearance of two new bands at 1515 and 1448 cm^{-1} compared to that of AAC, which are characteristic of the acidity provided by the titanium hydroxides inserted into acidified bentonite matrix. The 5V/Ti-AAC material still shows the presence of the four bands, indicating the Brønsted, Brønsted/ Lewis, and Lewis acid sites.

The Brønsted and Lewis acid sites were estimated by calculating the area of the *Peakfit* absorption bands, then these areas were used to quantify the acid sites (Table 3). These results show that the acid-activated bentonite exhibits a Brønsted acidity which decreased after intercalation of the titanium, although the Lewis acidity does not appear until after the introduction of the titanium. After impregnation with vanadium, a slight decrease in Brønsted acidity was recorded with the reappearance of the four acidity bands.

The morphology of various samples examined via SEM coupled with EDX (Fig. 5) found large particle aggregates with smooth surfaces in the AAC sample, while the 5V/Ti-AAC sample showed the formation of disordered structures at the end of the delamination process, in accordance with XRD results. The EDX results confirmed the presence of Ti and V after intercalation.

Catalytic activity

Here the oxidation of cyclohexene proceeds through two distinct pathways. The first pathway involves a direct epoxidation process

Table 3. Lewis and Brønsted acid sites accessible to pyridine used as probe molecules estimated by the FTIR integrated bands area

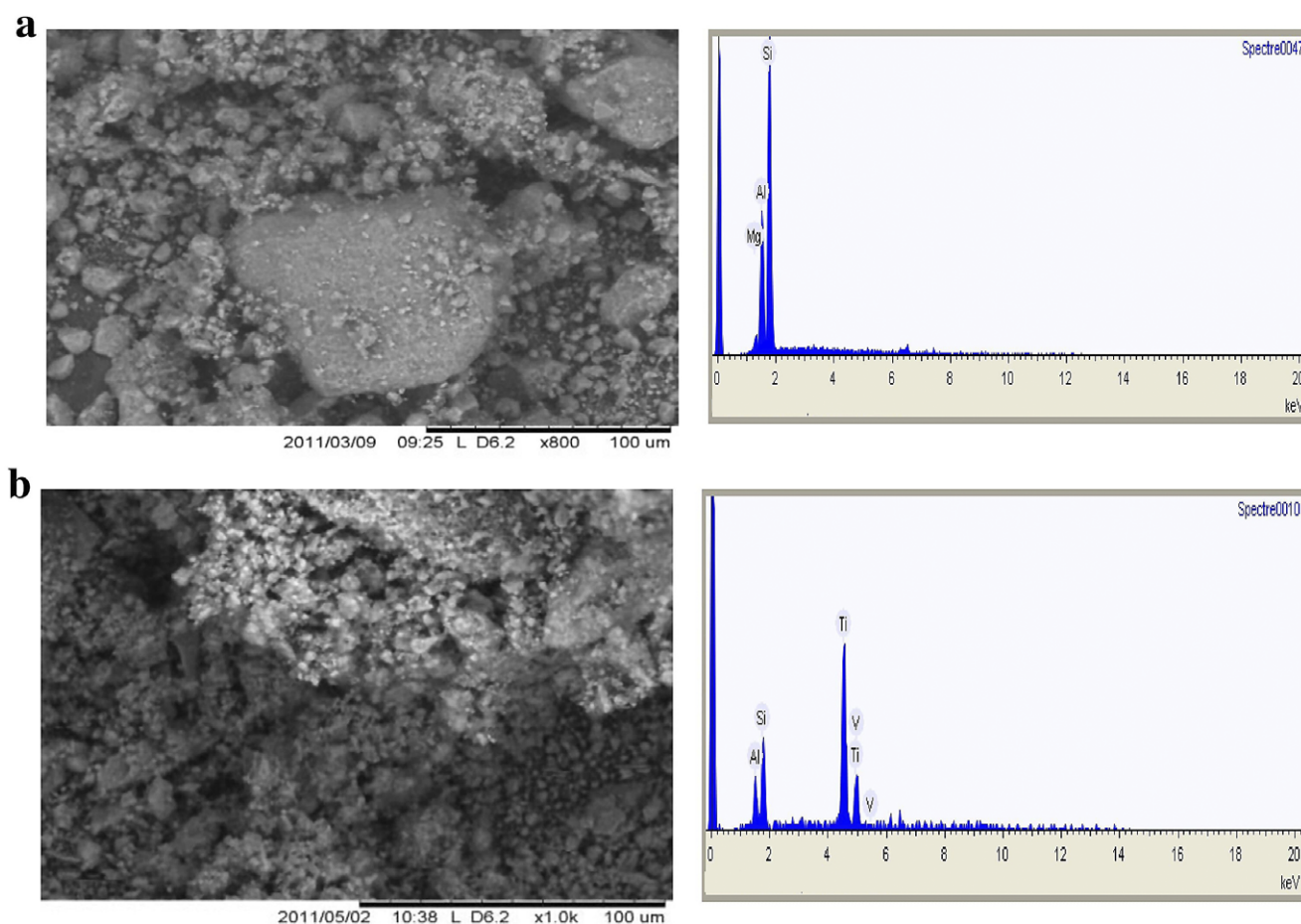| Materials	Brønsted sites (band at 1545 cm^{-1})	Brønsted sites (band at 1515 cm^{-1})	L/B Sites (band at 1490 cm^{-1})	Lewis sites (band at 1448 cm^{-1})
Raw clay	–	–	–	–
AAC	0.6622		0.3184	–
Ti-AAC	0.4010	0.2347	0.1467	0.0586
5V/Ti-AAC	0.5397	0.4317	0.1822	0.1283

Figure 5. SEM images and EDX analysis of (a) AAC and (b) 5V/Ti-AAC.

facilitated by redox catalysts, leading to the formation of the epoxide product. On the other hand, the second pathway involves an allylic oxidation mechanism in the presence of Lewis acid catalysts, resulting in the formation of cyclohexenol, cyclohexenone, cyclohexanone, and cyclohexanol as products (Azzi et al., 2019). As is well known, the VO_x active species have a significant impact on the catalytic performance of vanadium-supported catalysts due to the presence of surface redox as well as acid sites (El-Korso et al., 2014).

Initially, the catalytic performance of the 5V/Ti-AAC catalyst was investigated in the epoxidation reaction of cyclohexene, using tert-butyl hydroperoxide TBHP as the oxidant, and heptane and acetonitrile as solvents. The conversion, selectivity, and TOF of the studied reaction are calculated using equations 1, 2, and 3

respectively. The results obtained are presented in Table 4. Both the support AAC and Ti-AAC exhibited low activity toward cyclohexene epoxidation, with minimal TBHP consumption. However, the impregnation of Ti-AAC with vanadium resulted in excellent catalytic activity, primarily yielding the epoxide as the major product. This enhancement in catalytic performance can be attributed to the presence of weak acid sites (Table 4) and the strong interaction between vanadium and titanium in the 5V/Ti-AAC catalyst (Comite et al., 2003; El-Korso et al., 2014). It can also be explained by the high redox potentials of Ti^{4+}/Ti^{3+} (2.5 V) and V^{5+}/V^{4+} (4.5 V) couples (Nanjundaswamy et al., 1996; Patoux and Masquelier, 2002).

Moreover, it was observed that the use of acetonitrile as the solvent led to a greater conversion of cyclohexene (34%) compared

Table 4. Epoxidation of cyclohexene using different solvents

Catalysts	Amount of acid sites ($\mu mol\ g^{-1}$)		Heptane					Acetonitrile				
	Lewis acid sites	Brønsted acid sites	TBHP Consumption (%)	Activity		Selectivity (%)		TBHP Consumption (%)	Activity		Selectivity (%)	
				Conv. (%)	TOF (h^{-1})	Epoxide	others		Conv. (%)	TOF (h^{-1})	Epoxide	others
AAC	0	7	8	0	0	0	0	7	0	0	0	0
Ti-AAC	1	4	10	0	0	0	0	9	0	0	0	0
5V/Ti-AAC	1	6	44	26	8. 6	68	32	60	34	4. 5	27	73

Reaction conditions. cyclohexene 29 mmol, TBHP 38.45 mmol, solvent 25 mL, 0.1 g catalyst, 6 h, reaction temperature 65°C.

to heptane (26%). However, this change in the solvent resulted in a significant decrease in the selectivity of cyclohexene epoxide, with almost half of the desired product being lost. These results suggest that acetonitrile tends to favor the oxidation pathway rather than the epoxidation pathway, possibly due to the solvent covering the intermediate sites formed between TBHP and vanadium oxide. Similar observations were reported by Ouidri et al. (2010). This phenomenon can be attributed to the hydrophobic nature of the clay intercalated by titanium. The support exhibits a strong affinity for cyclohexene due to the reduction in polarity on its surface caused by the intercalation process, resulting in the generation of a hydrophobic surface (Shimizu et al., 2002). The polar solvent, acetonitrile, serves as a transporter, facilitating the entry of cyclohexene molecules from the external environment into the catalyst pores. Within these pores, the oxidation reaction occurs on active catalytic sites containing one or more vanadium atoms. Conversely, in the case of heptane, the affinity for the materials prepared is considerably weaker due to its lower polarity and uncharged nature. These factors collectively account for the greater conversion rates observed with acetonitrile compared to heptane. Acetonitrile's polar nature promotes a stronger interaction with the catalytic support, leading to changes in the size and shape of the pores. Consequently, this alteration results in a reduced selectivity toward the epoxidation reaction. To address this concern, heptane is employed as the solvent for subsequent studies. The use of heptane as a solvent helps to maintain the desired selectivity while maintaining acceptable conversion rates.

Based on the findings presented in Table 5, the quantity of catalyst significantly impacts the conversion of cyclohexene, with values ranging from 26% to 18% as the catalyst mass varied from 100 mg to 30 mg. This variation could be attributed to the reduction in active vanadium sites at lower catalyst masses. Conversely, a slight improvement in epoxide selectivity was observed when using a 30 mg 5V/Ti-AAC catalyst. Furthermore, increasing the catalyst

amount to 150 mg led to a substantial increase in cyclohexene conversion from 26% to 46%. However, it also resulted in a sharp decline in epoxide selectivity from 68% to 39%. This phenomenon is explained by the synergistic effect of vanadium sites acting as active sites, which intensifies with greater catalyst mass. To strike a balance between conversion and selectivity, the subsequent study will be conducted using 100 mg of catalyst.

The cyclohexene epoxide selectivity is also influenced by the quantity of TBHP which is another important parameter. To explore this, the effect of the amount of TBHP was examined while keeping the cyclohexene substrate constant. Various cyclohexene to TBHP molar ratios were tested, ranging from 1.3 to 3, using 100 mg of 5V/Ti-AAC catalyst. As indicated in Table 6, increasing the amount of oxidant does not have a significant impact on the selectivity of reaction products; the selectivity remained unchanged for cyclohexene epoxide and underwent minor changes for other byproducts. This finding aligns with a similar result reported by Kumaresan et al. (2010). Conversely, an elevation in the TBHP/cyclohexene molar ratio led to a direct increase in cyclohexene conversion. This phenomenon can be attributed to the alteration of the hydrophilic/hydrophobic balance in the reaction medium caused by the addition of TBHP, which possesses a hydrophilic nature. Based on the catalytic experimental results and in line with findings from various literature sources, the observed increase in cyclohexene conversion can be attributed to the change in the solvent environment due to the hydrophilic nature of TBHP (Farzaneh et al., 2004; Sedighipoor et al., 2017; Su et al., 2014).

The proposed mechanism for the reaction (Fig. 6) reveals that the vanadium (+V) forms a complex with TBHP, resulting in an intermediate metal peroxide complex. Subsequently, cyclohexene interacts with one of the metal-peroxo bonds, leading to the formation of the peroxo metallocycle. The peroxo-metallocycle undergoes a breakage process, generating cyclohexene oxide,

Table 5. Effect of the amount of catalyst on the cyclohexene epoxidation

| Catalyst amount (mg) | Activity (%) | | TBHP Consumption (%) | Selectivity (%) | | | | |
	Conv. (%)	TOF (h^{-1})		Epoxide	One	Enone	Enol	Diol
30	18	21.0	28	71	10	8	11	/
50	22	13.9	35	64	14	10	12	/
75	23	8.8	37	58	15	13	14	/
100	26	8.7	44	68	10	9	13	/
150	46	5.9	48	39	22	16	23	/

Reaction conditions. Cyclohexene 29 mmol, TBHP 38.45 mmol, Heptane 25 mL, 6 h, reaction temperature 65°C.

Table 6. Effect of TBHP/Cyclohexene molar ratio on the cyclohexene epoxidation

| TBHP/cyclohexene | Activity | | TBHP Consumption (%) | Selectivity (%) | | | | |
	Conv. (%)	TOF (h^{-1})		Epoxide	One	Enone	Enol	Diol
1.3	26	8.7	44	68	10	9	13	/
2	33	11.2	43	69	19	9	3	/
3	42	14.1	54	68	25	7	/	/

Reaction conditions: cyclohexene 29 mmol, Heptane 25 mL, 0.1 g catalyst, 6 h, reaction temperature 65°C.
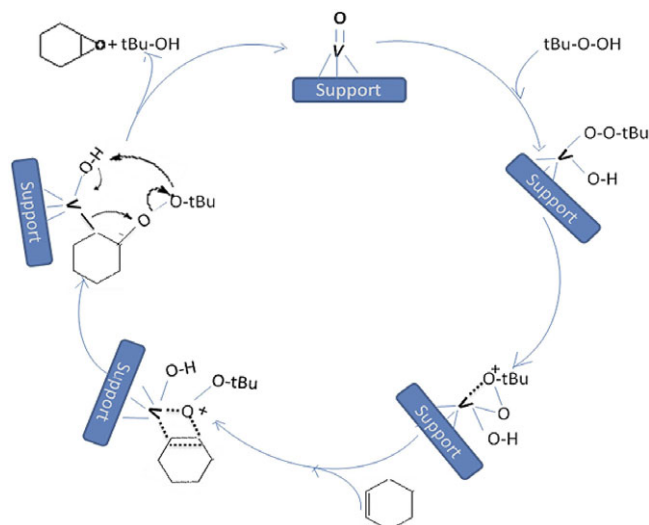
Figure 6. Proposed mechanism of epoxidation of cyclohexene over the 5V/Ti-AAC catalyst.

while the 5V/Ti-AAC catalyst is regenerated to initiate a new reaction cycle. Furthermore, the catalytic performance of the 5V/Ti-AAC catalyst was compared to that reported in the literature for cyclohexene epoxidation. The results demonstrate that the 5V/Ti-AAC material ranks among the most active catalysts (Table 7).

The variation of cyclohexene conversion with reaction time at three different temperatures (60°C, 70°C, and 80°C) is illustrated in Fig. 7. The present kinetic study aimed to determine the activation energy of the epoxidation reaction of cyclohexene using the 5V/Ti-AAC catalyst. The reaction conditions included a TBHP/Cyclohexene molar ratio of 3 and a catalyst mass of 100 mg. Furthermore, the decrease in selectivity toward cyclohexene epoxide with increasing reaction temperature is noted (Fig. 8).

The rate of the epoxidation reaction of cyclohexene is written as follows:

$$r = k * [C_6H_{10}]^{\alpha} * [TBHP]^{\beta} \qquad (4)$$

and

$$r = -d(C_6H_{10})/d(t) \qquad (5)$$

where α is partial order related to cyclohexene; β is partial order related to TBHP; t is time of reaction; and k is the rate constant of the reaction.

In order to discover reaction order, α, the authors assumed $[TBHP]^{\beta}$ to be constant because it is in excess, therefore:

$$r = k' * [C_6H_{10}]^{\alpha} \qquad (6)$$

Then:

$$-\frac{d(C_6H_{10})}{d(t)} = k' * [C_6H_{10}]^{\alpha} \qquad (7)$$

where k′ is the rate constant of the reaction.

In the present work, the reaction was assumed to have an order of 2 related to cyclohexene. For that reason, the integration of the equation 7 is:

$$\frac{1}{C} = k' * t + 1/C_0$$

where C is the cyclohexene concentration at given time t; and C_0 is the initial cyclohexene concentration.

To establish the kinetic order of the cyclohexene epoxidation reaction over the 5V/Ti-AAC catalyst, the reciprocal of concentration ($1/C$) was plotted against the reaction time at various reaction temperatures. The linearity of each equation (Fig. 9), proves that the reaction follows a kinetic order of 2.

R^2 coefficients are ~1 for the three plots and are straight lines which prove that the reaction of epoxidation of cyclohexene has a

Table 7. Comparison of the present work with literature

| Catalyst	Reaction conditions	Activity conv. %	Epoxide select. %	Reference
HWS-1_2/1	0.05 g catalyst, 10 mmol cyclohexene, 10 mmol CH_3CN, 10 mmol H_2O_2 (30 wt.%), $T = 60°C$, time = 2 h	11.8	82.2	(Wang et al., 2021)
WSn-MFI-a Sn-MFI-I	0.30 g catalyst, 20 mmol cyclohexene, 5 mL acetonitrile, 40 mmol H_2O_2 (30 wt.%,), $T = 65°C$, time = 9 h	93.3	85.6	(Zhang et al., 2020)
		33	89.7	
10 MeTiMCM-41	0.05 g catalyst, 5 mL acetonitrile, 10 mmol cyclohexene, 20 mmol of H_2O_2, $T = 60°C$, time= 7 h	38.8	68.7	(Kumar Roy et al., 2018)
Au/TiO$_2$ reduced	0.10 g catalyst, 4 mL cyclohexene, 5.5 mL [TBHP (70%) in water], $T = 70°C$, time = 6 h	58.4	20.2	(Ameur et al., 2013)
α-TiMnAs	catalyst (α-TiMAs, 0.2 mmol), 20 mmol cyclohexene, 4 mmol TBHP, 10 mL benzene, $T = 80°C$, time = 4 h	18.6	86.1	(Khare and Shrivastava, 2004)
Ti-montmorillonite	0.05 g catalyst, cyclohexene 20 mL, Ti-montmorillonite, UV irradiation and oxygen flow rate 100 mL/min	40	40	(Ouidri et al., 2010)
[Cu(sal-1,3-phen)]	0.10 g catalyst, 10 mmol cyclohexene, 16 mmol TBHP (solution 80% in di-*tert*-butylperoxide), 25 mL dichloromethane, $T = 80°C$, time = 8 h, under N_2 atmosphere	41.4	16.4	(Salavati-Niasari et al., 2007)
17. 5V16P/Al	2 mol.% catalyst, 20 mmol cyclohexene, 20 mmol TBHP (solution 80% in di-*tert*-butylperoxide /water 3:2), $T = 60°C$, time = 5 h	44	35	(Mikolajska et al., 2012)
5V/Ti-AAC	100 mg catalyst; TBHP/cyclohexene = 3; $T = 65°C$; n-heptane = 20 mL time = 6 h	42	68	Present study
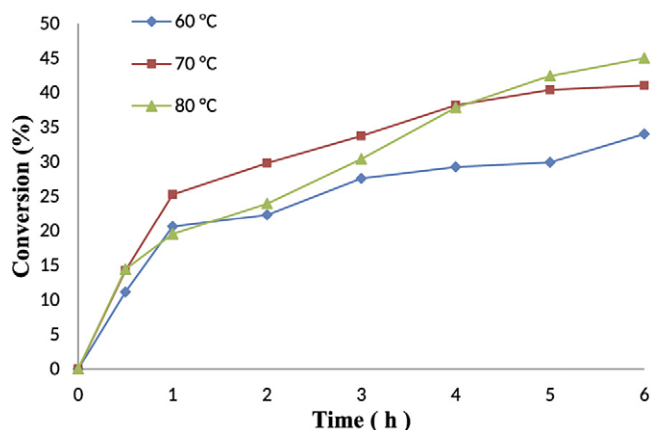
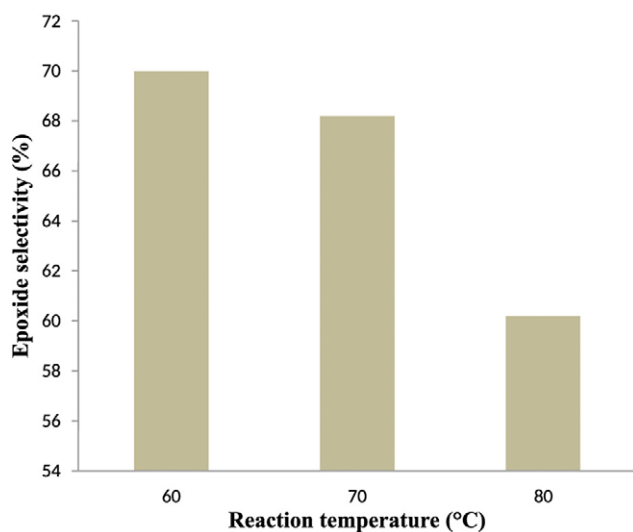**Figure 7.** Epoxidation reaction of cyclohexene as a function of temperature.

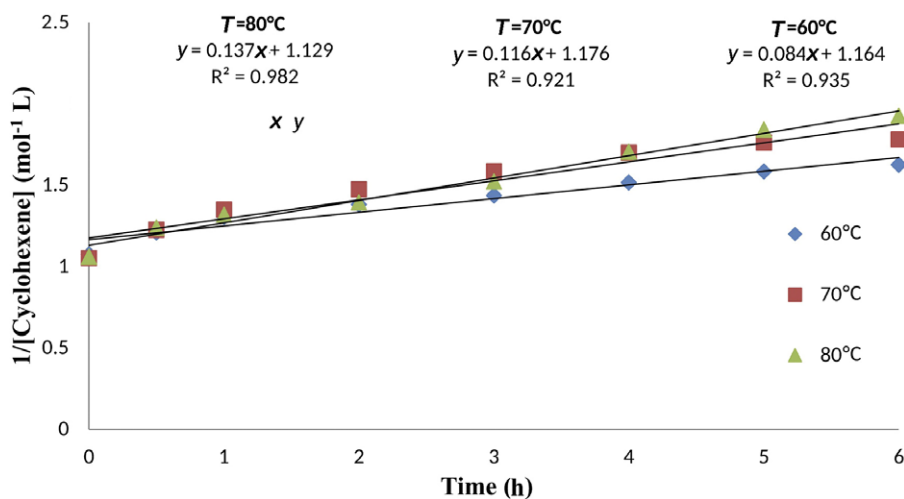**Figure 8.** Epoxide selectivity as function of reaction temperature.

Table 8. Rate constant value as a function of reaction temperature

T (°C)	T (K)	k	Ln (k)	$1/T$
60	333	0.084	−2.477	0.0030
70	343	0.116	−2.154	0.0029
80	353	0.137	−1.988	0.0028

kinetic order of 2. The calculated rate constant for each reaction temperature test is shown in Table 8.

According to the Arrhenius equation:

$$k = A * \exp\left(-\frac{E_a}{RT}\right)$$

$$\ln(k) = \ln(A) - E_a/RT$$

where k is the activation energy, A is the pre-exponential factor, E_a is the activation energy, R is the universal gas constant and T is the absolute temperature.

To calculate activation energy, $-\ln(k)$ was plotted versus $1/T$ (Fig. 10).

According to the tendency curve we have: $\frac{E_a}{R} = 2883$ with R = 8.314 kJ kmol^{-1} K^{-1}. So, the value of the activation energy will be:

$$E_a = 23.97 \, kJ \, mol^{-1}$$

The activation energy of the cyclohexene epoxidation over 5V/Ti-AAC is among the lowest energy in the literature (Kwon et al., 2015).

The stability of the catalyst is a crucial parameter that determines its potential for multiple reuses in consecutive reaction runs under identical conditions. To investigate the stability of the 5V/Ti-AAC catalyst in the cyclohexene epoxidation reaction, we conducted reusability tests for three reaction runs. After each run, the catalyst was separated from the reaction mixture via simple filtration. Subsequently, the catalyst was washed multiple times with the reaction solvent and dried at room temperature to prepare it for the next reaction run. The results of the catalyst reusability tests (Table 9) indicate a slight
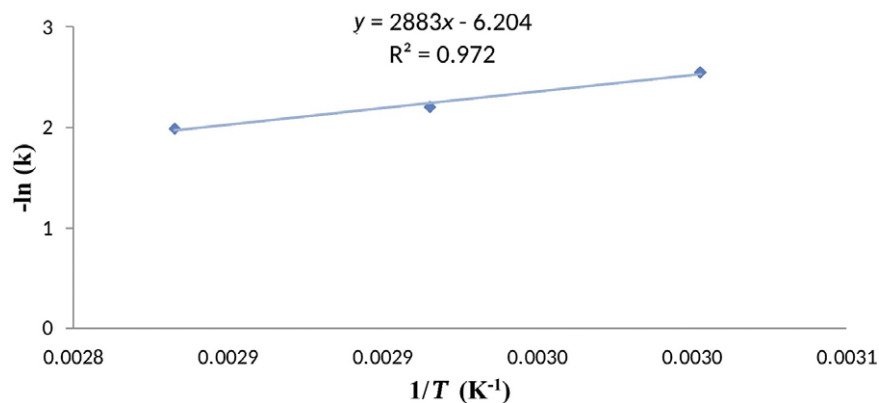

Figure 9. Kinetic data at various temperatures for the epoxidation of cyclohexene.

Figure 10. Arrhenius plot of the epoxidation of cyclohexene.

Table 9. Catalyst stability reaction tests

Run	Conversion (%)	TBHP consumption (%)	Epoxide selectivity (%)
1st	42	54	68
2nd	38	65	65
3rd	37	70	62

decrease in both reaction conversion and epoxide selectivity after three reaction runs. This observation can be attributed to the loss of catalyst during the recovery process after each reaction run. Despite the slight reduction in performance, the catalyst demonstrated promising reusability potential for multiple reaction cycles.

The recovered reaction mixtures were tested under the same reaction conditions by adding a quantity of cyclohexene in order to determine the vanadium leaching. The result shows no production of epoxide or byproducts as found by Brutchey et al. (2005) and Farzaneh et al. (2004).

Summary and conclusions

This investigation focused on exploring the potential of vanadium oxide-supported acid-modified clay (Ti-AAC) materials as catalysts for the environmentally friendly cyclohexene epoxidation reaction. The synthesized 5V/Ti-AAC material exhibited a mesoporous structure with introduced Lewis acidity through the incorporation of titanium into the clay matrix. Detailed analysis, including DR UV-vis, confirmed the presence of octahedral titanium in the anatase form and the existence of vanadium (+V) in the form of polymeric species V-O-V. The catalytic performance of 5V/Ti-AAC was exceptional, achieving a cyclohexene conversion of 42% with an impressive epoxide selectivity of 68%. These encouraging results were achieved under specific conditions, including a TBHP/cyclohexene molar ratio of 3, 100 mg of catalyst, and a reaction temperature of 65°C. Notably, the redox centers in the catalyst played a crucial role in directing the reaction toward epoxidation, surpassing the contribution of acid sites. The kinetic study revealed that the cyclohexene epoxidation reaction followed a second-order reaction with activation energy of 23.97 kJ mol^{-1}. This value surpassed various reported activation energies in previous research, indicating the catalyst's efficiency and potential for industrial applications. In addition, the reusability of the 5V/Ti-AAC catalyst demonstrated remarkable stability. It maintained its catalytic efficacy throughout three consecutive reaction runs, showcasing the potential for multiple cycles without significant loss in epoxide selectivity. Finally, this study developed successfully a highly efficient, environmentally friendly, and reusable 5V/Ti-AAC catalyst for the cyclohexene epoxidation reaction. The catalyst's excellent performance and stability make it a promising candidate for sustainable and economically viable epoxidation processes in industrial applications.

Competing interests. The authors declare no competing interests.

References

Ameur, N., Bedrane, S., Bachir, R., & Choukchou-Braham, A. (2013). Influence of nanoparticles oxidation state in gold based catalysts on the product selectivity in liquid phase oxidation of cyclohexene. *Journal of Molecular Catalysis A: Chemical*, 374-375, 1–6.

Arfaoui, J., Khafallah Boudali, L., & Ghorbel, A. (2006). Vanadia-doped titanium-pillared clay: Preparation, characterization and reactivity in the epoxidation of allylic alcohol (E)-2-hexen-1-ol. *Catalysis Communications*, 7, 86–90.

Arfaoui, J., Boudali, L. K., Ghorbel, A., & Delahay, G. (2009). Effect of vanadium on the behaviour of unsulfated and sulfated Ti-pillared clay catalysts in the SCR of NO by NH$_3$. *Catalysis Today*, 142(3-4), 234–238.

Arfaoui, J., Boudali, L. K., & Ghorbel, A. (2010). Catalytic epoxidation of allylic alcohol (E)-2-Hexen-1-ol over vanadium supported on unsulfated and sulfated titanium pillared montmorillonite catalysts: Effect of sulfate groups and vanadium loading. *Applied Clay Science*, 48(1-2), 171–178.

Azzi, H., Bendahou, K., Cherif-Aouali, L., Hamidi, F., Siffert, S., Bengueddach, A., & Aboukais, A. (2012). Total oxidation of toluene over Pd/mesoporous materials catalysts. *Chimica Oggi-Chemistry Today*, 30(4), 28–30.

Azzi, H., Rekkab-Hammoumraoui, I., Chérif-Aouli, L., & Choukchou-Braham, A. (2019). Mesoporous Co$_3$O$_4$ as a new Catalysts for allylic Oxidation of Cyclohexene *Bulletin of Chemical Reaction Engineering & Catalysis*, 14(1), 112–123.

Azzi, H., Chérif, L., & Siffert, S. (2020). Gold catalysts supported on cerium-modified mesoporous zirconia for total toluen oxidation. Effect of Ce/Zr molar ratio. *Research on Chemical Intermediates*, 47(3), 1009–1019.

Bahranowski, K., Dula, R., Komorek, J., Romotowski, T., & Serwicka, E. M. (1995). Preparation, physicochemical characterization and catalytic properties of vanadium-doped alumina- and titania-pillared montmorillonites. In: *Studies in Surface Science and Catalysis. Elsevier*, 91 (Poncelet, G., Martens, J., Delmon, B., Jacobs, P.A., and Grange, P., editors) pp. 747–754.

Bahranowski, K., Janas, J., Machej, T., Serwicka, E. M., & Vartikian, L. A. (1997). Vanadium-doped titania-pillared montmorillonite clay as a catalyst for selective catalytic reduction of NO by ammonia. *Clay Minerals*, 32(4), 665–672.

Bahranowski, K., Grabowski, R., Grzybowska, B., Kielski, A., Serwicka, E. M., Wcisło, K., Wodnicka, K. (2000). Synthesis and physicochemical properties of vanadium-doped zirconia-pillared montmorillonites in relation to oxidative dehydrogenation of propane. *Topics in Catalysis*, 11/12, 255–261.

Bailey, S. W., Brindley, G. W., & Brown, G., editors (1980) *Structures of Clay Minerals and their X-ray Identification*. Mineralogical Society, London.

Bardestani, R., Patience, G. S., & Kaliaguine, S. (2019). Experimental methods in chemical engineering: specific surface area and pore size distribution measurements—BET, BJH, and DFT. *The Canadian Journal of Chemical Engineering*, 97(11), 2781–2791.

Belaidi, N., Bedrane, S., Choukchou-Braham, A., & Bachir, R. (2015). Novel vanadium-chromium-bentonite green catalysts for cyclohexene epoxidation. *Applied Clay Science*, 107, 14–20.

Bineesh, K. V., Cho, D. R., Kim, S. Y., Jermy, B. R., & Park, D. W. (2008). Vanadium-doped titania-pillared montmorillonite clay for the selective catalytic oxidation of H_2S. *Catalysis Communications*, 9, 2040–2043.

Bineesh, K. V., Kim, S.-Y., Jermy, B. R., & Park, D.-W. (2009). Catalytic performance of vanadia-doped titania-pillared clay for the selective catalytic oxidation of H_2S. *Journal of Industrial and Engineering Chemistry*, 15(2), 207–211.

Bineesh, K. V., Kim, D.-K., Kim, D.-W., Cho, H.-J., & Park, D.-W. (2010a). Selective catalytic oxidation of H_2S to elemental sulfur over V_2O_5/Zr-pillared montmorillonite. *Energy & Environmental Science*, 3, 302–310.

Bineesh, K. V., Kim, D.-K., & Park, D.-W. (2010b). Synthesis and characterization of zirconium-doped mesoporous nano-crystalline TiO_2. *Royal Society of Chemistry/ Nanoscale*, 2, 1222–1228.

Bineesh, K. V., Kim, D.-K., Kim, M.-I., & Park, D.-W. (2011). Selective catalytic of H_2S over V_2O_5 supported on TiO_2-pillared clay catalysts in the presence of water and ammonia. *Applied Clay Science*, 53, 204–211.

Brutchey, R. L., Mork, B. V., Sirbuly, D. J., Yang, P., & Tilley, T. D. (2005). A dimeric molecular precursor [(^{t}BuO)$_2$Ti{μ-O$_2$Si[OSi(O^{t}Bu)$_3$]$_2$}]$_2$ to Ti(IV)/SiO$_2$ catalysts for selective cyclohexene epoxidation. *Journal of Molecular Catalysis A: Chemical*, 238(1-2), 1–12.

Candan Karaeyvaz, M., & Balci, S. (2021). One pot synthesis of aluminum pillared intercalated layered clay supported silicotungstic acid (STA/Al-PILC) catalysts. *Microporous and Mesoporous Materials*, 323, 111193.

Centi, G., & Perathoner, S. (2008). Catalysis by layered materials: A review. *Microporous and Mesoporous Materials*, 107(1-2), 3–15.

Chae, H. J., Nam, I.-S., Ham, S.-W., & Hong, S. B. (2004). Characteristics of vanadia on the surface of V_2O_5/Ti-PILC catalyst for the reduction of NO$_x$ by NH$_3$. *Applied Catalysis B: Environmental*, 53(2), 117–126.

Chaker, H., Fourmentin, S., & Chérif-Aouali, L. (2020). Efficient Photocatalytic Degradation of Ibuprofen under Visible Light Irradiation Using Silver and Cerium Co-Doped Mesoporous TiO_2. *Chemistry Select*, 5(38), 11787–11796.

Chary, V. R., Kumar, C. P., Naresh, D., Bhaskar, T., & Sakata, Y. (2006). Characterization and reactivity of Al_2O_3–ZrO_2 supported vanadium oxide catalysts. *Journal of Molecular Catalysis A: Chemical*, 243(2), 149–157.

Chen, D., Zhu, Q., Zhou, F., Deng, X., & Li, F. (2012). Synthesis and photocatalytic performances of the TiO2 pillared montmorillonite [Research Support, Non-U.S. Gov't]. *Journal of Hazardous Materials*, 235-236, 186–193.

Chitnis, S. R., & Sharma, M. M. (1997). Industrial applications of acid-treated clays as catalysts. *Reactive & Functional Polymers*, 32, 93–115.

Ciesielski, H., & Sterckeman, T. (1997). Determination of cation exchange capacity and exchangeable cations in soils by means of cobalt hexamine trichloride. Effects of experimental conditions. *Agronomie: Agriculture and Environment*, 17, 1–7.

Comite, A., Sorrentino, A., Capannelli, G., Di Serio, M., Tesser, R., & Santacesaria, E. (2003). Oxidative dehydrogenation of propane using V_2O_5/

TiO$_2$/SiO$_2$ catalysts prepared by grafting titanium and vanadium alkoxides on silica. *Journal of Molecular Catalysis A: Chemical*, 198(1-2), 151–165.

Concepcion, P., Navarro, M., Blasco, T., Lopeznieto, J., Panzacchi, B., & Rey, F. (2004). Vanadium oxide supported on mesoporous Al_2O_3 Preparation, characterization and reactivity. *Catalysis Today*, 96(4), 179–186.

El-Korso, S., Khaldi, I., Bedrane, S., Choukchou-Braham, A., Thibault-Starzyk, F., & Bachir, R. (2014). Liquid phase cyclohexene oxidation over vanadia based catalysts with tert-butyl hydroperoxide: Epoxidation versus allylic oxidation. *Journal of Molecular Catalysis A: Chemical*, 394, 89–96.

El-Korso, S., Bedrane, S., Choukchou-Braham, A., & Bachir, R. (2015). The effect of redox properties of ceria-supported vanadium oxides in liquid phase cyclohexene oxidation. *RSC Advances*, 5, 63382–63392.

El-Korso, S., Bedrane, S., Choukchou-Braham, A., & Bachir, R. (2016). Investigation of the effect of VO$_x$/ZrO$_2$ structure on the catalytic activity in cyclohexene epoxidation. *RSC Advances*, 6, 110375–110382.

Farzaneh, F., Zamanifar, E., & Williams, C. D. (2004). V-MCM-41 as selective catalyst for epoxidation of olefins and trans-2-hexene-1-ol. *Journal of Molecular Catalysis A: Chemical*, 218(2), 203–209.

Gao, J., Chen, Y., Han, B., Feng, Z., Li, C., Zhou, N., Xi, Z. (2004). A spectroscopic study on the reaction-controlled phase transfer catalyst in the epoxidation of cyclohexene. *Journal of Molecular Catalysis A: Chemical*, 210(1-2), 197–204.

Held, A., Kowalska-Kuś, J., & Nowińska, K. (2012). Epoxidation of propene on vanadium species supported on silica supports of different structure. *Catalysis Communications*, 17, 108–113.

Huang, Q., Zuo, S., & Zhou, R. (2010). Catalytic performance of pillared interlayered clays (PILCs) supported CrCe catalysts for deep oxidation of nitrogen-containing COCs. *Applied Catalysis B: Environmental*, 95, 327–334.

Iannazzo, V., Neri, G., Galvagno, S., Di Serio, M., Tesser, R., & santacesaria, E. (2003). Oxidative dehydrogenation of isobutane over V2O5-based catalysts prepared by grafting vanadyl alkoxides on TiO$_2$-SiO$_2$ supports. *Applied Catalysis A: General*, 246(1), 49–68.

Khare, S., & Shrivastava, S. (2004). Epoxidation of cyclohexene catalyzed by transition-metal substituted α-titanium arsenate using tert-butyl hydroperoxide as an oxidant. *Journal of Molecular Catalysis A: Chemical*, 217, 51–58.

Komadel, P., & Madejová, J. (2006). Acid Activation of Clay Minerals. *Developments in Clay Science*, 1, Elsevier, Amsterdam, pp. 263–287.

Kumar Roy, S., Dutta, D., & Talukdar, A. K. (2018). Highly effective methylated Ti MCM-41 catalyst for cyclohexene oxidation. *Materials Research Bulletin*, 103, 38–46.

Kumaresan, L., Prabhu, A., Palanichamy, M., & Murugesan, V. (2010). Mesoporous Ti-KIT-6 molecular sieves: Their catalytic activity in the epoxidation of cyclohexene. *Journal of the Taiwan Institute of Chemical Engineers*, 41(6), 670–675.

Kwon, S., Schweitzer, N. M., Park, S., Stair, P. C., & Snurr, R. Q. (2015). A kinetic study of vapor-phase cyclohexene epoxidation by H_2O_2 over mesoporous TS-1. *Journal of Catalysis*, 326, 107–115.

Lippens, B. C., & De Boer, J. H. (1995). Studies on Pore Systems in Catalysts V. The t Method. *Journal of Catalysis*, 4, 319–323.

Long, R. Q., & Yang, R. T. (2000a). Catalytic Performance and Characterization of VO^{2+}-Exchanged Titania-Pillared Clays for Selective Catalytic Reduction of Nitric Oxide with Ammonia. *Journal of Catalysis*, 196(1), 73–85.

Long, R. Q., & Yang, R. T. (2000b). Selective catalytic reduction of NO with ammonia over V_2O_5 doped TiO$_2$-pillared clay catalysts. *Applied Catalysis B: Environmental*, 24, 13–21.

Mikolajska, E., Calvino-Casilda, V., & Bañares, M. A. (2012). Real-time Raman monitoring of liquid-phase cyclohexene epoxidation over alumina-supported vanadium and phosphorous catalysts. *Applied Catalysis A: General*, 421-422, 164–171.

Murgia, V., Torres, E. M. F., Gottifredi, J. C., & Sham, E. L. (2006). Sol–gel synthesis of V_2O_5–SiO_2 catalyst in the oxidative dehydrogenation of n-butane. *Applied Catalysis A: General*, 312, 134–143.

Najafi, H., Farajfaed, S., Zolgharnian, S., Mosavi Mirak, S. H., Asasian-Kolur, N., & Sharifian, S. (2021). A comprehensive study on modified-pillared clays as an adsorbent in wastewater treatment processes. *Process Safety and Environmental Protection*, 147, 8–36.

Nanjundaswamy, K. S., Padhi, A. K., Goodenough, J. B., Okadab, S., Ohtsukab, H., Araib, H., & Yamaki, J. (1996). Synthesis, redox potential evaluation and electrochemical characteristics of NASICON-related-3D framework compounds. *Solid State Ionics*, 92, 1–10.

Oubagaranadin, J. U. K., Murthy, Z. V. P., & Mallapur, V. P. (2010). Removal of Cu(II) and Zn(II) from industrial wastewater by acid-activated montmorillonite-illite type of clay. *Comptes Rendus Chimie*, *13*(11), 1359–1363.

Ouidri, S., Guillard, C., Caps, V., & Khalaf, H. (2010). Epoxidation of olefins on photoirradiated TiO_2-pillared clays. *Applied Clay Science*, *48*(3), 431–437.

Parida, K. M., & Mallick, S. (2009). Phosphotungstic acid promoted zirconia–alumina mixed oxides: A stable and reusable catalysts for epoxidation of trans-stilbene. *Catalysis Communications*, *11*(1), 51–57.

Patoux, S., & Masquelier, C. (2002). Lithium Insertion into Titanium Phosphates, Silicates, and Sulfates. *Chemicals Materials*, *14*, 5057–5068.

Pinnavaia, T. J. (1983). Intercalated clay catalysts. *Science*, *220*(4595), 365–371.

Rhodes, C. N., Franks, M., Parkes, G. M. B., & Brown, D. R. (1991). The effect of acid treatment on the activity of clay supports for $ZnCl_2$ alkylation catalysts. *Journal of the Chemical Society, Chemical Communications*, *12* (12), 804–807.

Salavati-Niasari, M., Shaterian, M., Ganjali, M. R., & Norouzi, P. (2007). Oxidation of cyclohexene with tert-butylhydroperoxide catalysted by host (nanocavity of zeolite-Y)/guest (Mn(II), Co(II), Ni(II) and Cu(II) complexes of N,N′-bis(salicylidene)phenylene-1,3-diamine) nanocomposite materials (HGNM). *Journal of Molecular Catalysis A: Chemical*, *261*(2), 147–155.

Sedighipoor, M., Kianfar, A. H., Mahmood, W. A. K., & Azarian, M. H. (2017). Epoxidation of alkenes by an oxidovanadium(IV) tetradentate Schiff base complex as an efficient catalyst with tert-butyl hydroperoxide. *Inorganica Chimica Acta*, *457*, 116–121.

Shimizu, K.-I., Kaneko, T., Fujishima, T., Kodama, T., Yoshida, H., & Kitayama, Y. (2002). Selective oxidation of liquid hydrocarbons over photoirradiated TiO2 pillared clays. *Applied Catalysis A: General*, *225*, 185–191.

Sreethawong, T., Yamada, Y., Kobayashi, T., & Yoshikawa, S. (2005). Catalysis of nanocrystalline mesoporous TiO_2 on cyclohexene epoxidation with H_2O_2: Effects of mesoporosity and metal oxide additives. *Journal of Molecular Catalysis A: Chemical*, *241*(1-2), 23–32.

Su, H., Li, Z., Huo, Q., Guan, J., & Kan, Q. (2014). Immobilization of transition metal (Fe^{2+}, Co^{2+}, VO^{2+} or Cu^{2+}) Schiff base complexes onto graphene oxide as efficient and recyclable catalysts for epoxidation of styrene. *RSC Advances*, *4*(20), 9990–9996.

Torres, M., de los Santos, C., Portugau, P., Yeste, M. D. P., & Castiglioni, J. (2021). Utilization of a PILC-Al obtained from Uruguayan clay as support of mesoporous MnOx-catalysts on the combustion of toluene. *Applied Clay Science*, *201*, 105935.

Wang, T., Zhu, R. L., Ge, F., Zhu, J. X., He, H. P., & Chen, W. X. (2010). Sorption of phenol and nitrobenzene in water by CTMAB/CPAM organobentonites. *Huan jing Ke xue/ Environmental Science*, *31*(2), 385–389.

Wang, X., You, Q., Wu, Y., Bi, C., Chen, H., Dai, C., Ma, X. (2021). Tungsten-substituted Silicate-1 with an interconnected hollow structure for catalytic epoxidation of cyclohexene. *Microporous and Mesoporous Materials*, *317*, 111028.

Yamanka, S., Nishihara, T., & Hattori, M. (1987). Preparation and properties of titania pillared clay. *Materials Chemistry and Physics,17*, 87–101.

Yuan, P., Yin, X., He, H., Yang, D., Wang, L., & Zhu, J. (2006). Investigation on the delaminated-pillared structure of TiO2-PILC synthesized by $TiCl_4$ hydrolysis method. *Microporous and Mesoporous Materials*, *93*(1-3), 240–247.

Zhang, H., Yang, X., Song, X., Chang, X., & Jia, M. (2020). Hydrothermal synthesis of tungsten-tin bimetallic MFI type zeolites and their catalytic properties for cyclohexene epoxidation. *Microporous and Mesoporous Materials*, *303*, 110277.